Radiationless Electromagnetic Interference: Diffractive Evanescent-Field Lenses and Perfect Focusing

R. Merlin

FOCUS Center and Department of Physics, The University of Michigan, Ann Arbor, MI 48109-1040

April 16, 2007

Planar subwavelength structures are described, which rely on a hitherto unrecognized property of Maxwell's equations to provide superlensing, i. e., electromagnetic focusing well beyond the diffraction limit, at arbitrary frequencies. The resulting fields bear a striking resemblance to those shown by negative-refraction slabs. The structures' design is related to that of the Fresnel plates in that diffraction forces the input field to converge to a spot on the focal plane. Unlike the diffraction-limited zone plates, for which focusing results from standard interference of traveling waves, the subwavelength plates control the near field and, as such, their superlensing properties originate from a new, static form of interference.

PACS numbers:

The closely related problems of electromagnetic imaging and focusing beyond Abbe's diffraction limit (set by ~ λ/n where λ is the vacuum wavelength and n is the refractive index [1]) have received considerable attention in the past decade, motivated in part by the optical studies of Betzig and Trautman [2], who used subwavelength apertures to probe the near field (for related work at microwave frequencies, see [3]). Since then, various schemes have been developed to improve the resolution, involving, e. g., sharp tips [4,5], tapered plasmonic waveguides [6] and far-field time reversal mirrors [7], and values as small as ~ $\lambda/100$ have been reported for the THz range [8]. Subwavelength focusing necessarily involves the evanescent components of the field, i. e., the near field. Because of this, standard interference techniques or geometrical optics methods do not apply. More recently, negative refraction has emerged as a new topic of interest to near-field studies [9,10], following Pendry's work on perfect lenses [11] (see also [12,13,14]), and the subsequent experimental verification of negative refraction at microwave frequencies [15,16] and imaging beyond Abbe's limit with negative-permittivity slabs [17,18]. In this work, a novel approach to subwavelength focusing is described which uses patterned, planar structures to induce convergence of the near field. The focusing effect described here is reminiscent of, but the physics is significantly different than that of, both, negative refraction slabs and Fresnel zone plates [19].

Let F be one of the cartesian components of the electric (**E**) or the magnetic field (**H**), and assume that all the field sources are monochromatic, with time-dependence given by $e^{-i\omega t}$ (ω is the angular frequency), and that they lie, say, to the left of a particular plane, defined as $z = 0$.

Then, for $z \geq 0$, F satisfies the Helmholtz equation $\nabla^2 F + k^2 F = 0$ and can thus be expressed in the angular-spectrum-representation form [20]

$$F(x, y, z_\alpha) = \frac{1}{4\pi^2} \int_{-\infty}^{+\infty} \iiint F(x', y', z_\beta) e^{i\left[q_x(x-x') + q_y(y-y') + \kappa(z_\alpha - z_\beta)\right]} dx' dy' dq_x dq_y \tag{1}$$

providing an exact relationship between the solution to the wave equation in two arbitrary planes, parallel to each other, $z = z_\alpha > 0$ and $z = z_\beta > 0$. Here, $k = 2\pi/\lambda$ and

$$\kappa = \begin{cases} i\left|\left(q_x^2 + q_y^2 - k^2\right)^{1/2}\right| & q_x^2 + q_y^2 \geq k^2 \\ \left|\left(k^2 - q_x^2 - q_y^2\right)^{1/2}\right| & q_x^2 + q_y^2 < k^2 \end{cases} . \tag{2}$$

With the sources located in the half-space $z < 0$, the choice of signs in (2) is dictated by the requirements that the homogeneous and inhomogeneous (or evanescent) solutions to the wave equation must travel and decay in the positive z direction, respectively.

Since, according to Eq. (1), the field in the region $z \geq 0$ is determined by the boundary values $F(x,y,0)$, the question of focusing (for, both, the subwavelength and the conventional, diffraction-limited cases) becomes that of identifying the sources needed to generate the field profile at $z = 0$ that converges to a spot of a predetermined size at the focal plane, $z = f$. While the angular-spectrum representation shows that $F(x,y,0)$ is, in turn, uniquely determined by the focal-plane values, $F(x,y,f)$, the answer to the focusing problem is not unique, and the search for the optimal solution is not trivial, because "focal spot" is, at best, an electromagnetically vague concept. The difficulty here is that the wrong choice of $F(x,y,f)$ may result in a field that is unsuitable for applications, diverges or does not exist (everywhere in a region or at certain points),

or a boundary field that is difficult to implement in practice. In our approach, $F(x,y,0)$ is defined by the transmission properties of subwavelength-patterned planar structures that behave, in some sense, like the evanescent-wave counterparts to Fresnel's zone plates [19]. Similar to the latter structures, the waves exit our plates in a pattern set by the plate design, which forces them to converge to a spot on the focal plane, as prescribed by Eq. (1). Unlike the Fresnel plates, which rely on interference involving radiative components of the field (and are thus subjected to Abbe's constraint), our plates affect primarily the evanescent waves leading to interference effects that are electrostatic or magnetostatic in nature and, as a result, the spot size can be arbitrarily small. As with other near-field effects, our plates' ability to focus at large distances is severely limited by the exponential decay of the near field which, in practical applications, constrains the focal length to dimensions much smaller than λ.

The plates we propose can be tailored to give subwavelength focal patterns of various types and symmetries. Here, we concentrate on two key geometries displaying cylindrical and azimuthal symmetry. In the cylindrical or two-dimensional case, $\partial F / \partial x = 0$, the perfect focus is a line and Eq. (1) becomes

$$F(y, z_\alpha) = \frac{1}{2\pi} \iint_{-\infty}^{+\infty} F(y', z_\beta) e^{i\left[q(y-y')+\kappa(z_\alpha - z_\beta)\right]} dy' dq \quad , \tag{3}$$

where $\kappa(q)$ is given by (2) with $q_x^2 + q_y^2 \to q^2$. For electromagnetic fields propagating in the $+z$ direction that have azimuthal symmetry (e. g., the axicon [21] and Bessel beams [22]), the tangential, ϕ-component of the electric field as well as the z- and the radial, ρ-component of **H** van-

ish, while the non-zero components $\Psi = H_\phi$ or E_ρ obey

$$\Psi(\rho, z_\alpha) = \int_{-\infty}^{+\infty}\int \Psi(\rho', z_\beta) J_1(q\rho') J_1(q\rho) e^{i\kappa(z_\alpha - z_\beta)} \rho' d\rho' q dq \quad . \tag{4}$$

Replacing the Bessel function J_1 by J_0, one obtains the corresponding expression for E_z. Note that $e^{iq_0 y}\exp[i\kappa(q_0)z]$ and $J_1(q_0\rho)\exp[i\kappa(q_0)z]$ are, respectively, solutions of (3) and (4) for arbitrary q_0, that become evanescent modes for $|q_0| > k$. For $|q_0| < k$, the corresponding fields are the well-known diffraction-free plane waves and Bessel beams. As discussed in the next paragraph, these states and, more generally, source-free electromagnetic fields with components of the form $f_{q_0}(\boldsymbol{\rho})\exp[i\kappa(q_0)z]$, where $\boldsymbol{\rho}$ is a vector normal to the z-axis, play a crucial role in near-field lensing.

Our approach to subwavelength focusing relies on a property of the near field which, to the best of our knowledge, has not been considered before. Assume that $f_{q_0}\exp[i\kappa(q_0)z]$ is part of a full solution to Maxwell's equations, and that a certain field component (cartesian or otherwise) at the source plane, $z = 0$, is of the form $M(\boldsymbol{\rho}) \times f_{q_0}(\boldsymbol{\rho})$ where M is a modulation function, which is characterized by the length scale L and satisfies the requirements specified below. Then, it can be shown for $|q_0| >> k$ that the field converges to a focal spot of resolution defined by $\ell = 2\pi/|q_0|$, after propagating through a distance of order L. This remarkable effect is illustrated in Fig. 1 for, both, the two-dimensional and azimuthally-symmetric cases. The basic concepts of near-field lensing are best understood in the cylindrical geometry. In Eq. (3), take $F(y,0) = M(y)e^{iq_0 y}$ and integrate to calculate $F(y,z)$. Since, for $|q_0| >> k$, the relevant states are

evanescent waves, we can approximate $\kappa(q) \approx i|q|$ so that $F(y,z) \approx \iint e^{iqy} e^{-|q|z} M(y') e^{i(q_0 - q)y'} dy' dq / 2\pi$. Lensing occurs for a wide choice of modulation functions. Mathematically, a sufficient condition for focusing is that M should have one or more poles in the complex plane with non-zero imaginary components. To prove this, we assume that $M(y)$ is a real and even function, with poles at $\pm iL$. Performing a simple integration, we obtain

$$F(y,z) \propto \left[\frac{e^{q_0(iy+L-z)} - 1}{iy + L - z} + \frac{(iy + L + z) e^{q_0(iy+L-z)} + (-iy + L + z)}{y^2 + (z+L)^2} \right] . \quad (5)$$

As anticipated, the first term of this expression leads to focusing at $z = L$ such that, for $L >> \ell$, $|F(y,L)|^2 \propto |\sin(q_0 y/2)/y|^2$ (the second term gives, comparatively, a weakly-varying background). A comment is in order here. Since there are no phases associated with evanescent waves, it should come as a surprise that the lensing process shows telltale signs of conventional interference, particularly in the way the waves contributing to (3) add up constructively and destructively at the focal plane. Because it involves nonradiative modes, we will refer to this unconventional form of focusing as radiationless interference.

Fig. 1A shows plots of $|F(y,z)|^2$, obtained from Eq. (3), for $f_{q_0} = e^{iq_0 y}$ and $M = (1 + y^2/L^2)^{-1}$. This form of M is the simplest one for an even function with poles at $y = \pm iL$. The calculations are consistent with Eq. (5), and support our contention that the focal length and the resolution are determined, respectively, by the modulation length, L, and the length scale of the unperturbed field component, ℓ. As shown in Fig. 1B, the modulated azimuthally-symmetric field (ring-like focus) exhibits a similar effect. Although our study has been so far limited to

simple poles located in the imaginary axis, it can be easily shown that (*i*) focusing can also be attained with higher-order poles, (*ii*) modulation functions with multiple poles give multiple foci, and (*iii*) the real and imaginary part of a given pole determine, respectively, the off-axis position of the focal spot and the corresponding focal length. Within this context, it is of interest to apply our analysis to a negative-refraction slab which exhibits perfect focusing at $n = -1$ [11]. For $|1+n| << 1$ and a source consisting of a line of dipoles, the expression for the field is known analytically [14]. In particular, if the slab thickness is d and the source is at a distance $d/2$ from the nearest slab surface (and, therefore, its image is at $d/2$ from the other surface [11]), the evanescent field at the exit side of the slab can be written as $M(y)e^{iq_0 y}$ where

$$M(y) \propto \frac{\cosh(\pi y/2d) - i\sinh(\pi y/2d)}{\cosh(\pi y/2d) + i\sinh(\pi y/2d)} \tag{6}$$

and $q_0 = -\ln|1+n|/d$ [14]. As expected, M exhibits a pole at $y = id/2$ reflecting the image location and, moreover, the expression for q_0 is in perfect agreement with the known slab resolution [14,23]. Since M has an infinite number of additional poles at $y = i(d/2 + 2pd)$, where $p > 0$ is an integer, a near-perfect slab will exhibit not just one, but an infinite number of images, for which the intensity decays exponentially with p.

For the two-dimensional geometry, the above results can be trivially extended from the simple sinusoidal to the general case of a periodic field $P_\ell(y)$, of period ℓ. It is apparent that, for values at the source plane given by $F(y,0) = M(y)P_\ell(y)$, the field will converge at $z = L$ to a focal spot of size $\sim \ell$. This suggests the path for a practical implementation of cylindrical near-field lensing. Since a periodic field can be simply realized by letting a plane wave go

through an array of periodically-placed slits (or ribbons), it is clear that a field of the form $M(y)P_\ell(y)$ can be obtained by introducing a slowly-varying modulation in, say, the width or the properties of the material an element is made of. Similarly, in the case of azimuthal symmetry, a Bessel beam can be used together with a set of concentric rings of properly-modulated width placed, say, at radii satisfying $J_1(q_0\rho)=0$. The technology for manufacturing plates of this kind for microwave applications has been available for quite some time, while nanofabrication methods involving, say, focused ion beam lithography, can be used for the infrared and optical range. An important consideration in the design of a near-field plate is to avoid as much as possible the presence of terms, such as the second one of (5), giving a background that could overwhelm the sharp features of the field. An example of background-free focusing is shown in Fig. 2. These results are for the diffraction of a plane wave by a set of ribbons of very narrow width $<< \ell$ and parameters such that the total current density is $\mathbf{j} = (j_x,0,0)$ where

$$j_x \propto \delta(z)\sum_{s=-\infty}^{\infty}\frac{(-1)^s\delta(y-s\ell)}{\left(1+s^2\ell^2/L^2\right)} \tag{7}$$

(the incident electric field is parallel to the cylindrical axis). Such an array of currents, with the sign varying from one element to the next, can be realized at infrared and optical frequencies by alternating material with positive and negative permittivity and, in the microwave regime, by using a set of interchanging capacitive and inductive elements. Fig. 2B shows a contour plot of the y-component of the diffracted magnetic field (logarithmic scale). These results are remarkably similar to those reported for negative-refraction slabs [14,24], thereby revealing the close relationship between both phenomena. Finally, to help ascertain the origin of radiationless interfer-

ence, we show in Fig. 2C a linear plot of the field intensity, normalized to its largest value at a given z. The figure clearly shows behavior suggestive of beam coupling in that the diffraction of the beam produced by a particular current source is prevented by the presence of its neighbors. It is only after the intensity of its neighbors has decreased a sufficient amount that the central beam is allowed to spread, and the point at which this happens determines the focal length.

In summary, we have shown that near-field focusing can be achieved by modulating an evanescent state, that is itself a solution to Maxwell's equations. The process by which subwavelength focusing is attained is a new, radiationless form of interference. We further showed that this effect is closely related to lensing by negative refraction slabs, and proposed a practical implementation utilizing planar structures whose design is related to that of Fresnel zone plates.

The author acknowledges discussions with A. Grbic. This work was supported by the Air Force Office of Scientific Research under contract FA 9550-06-01-0279 through the Multidisciplinary University Research Initiative Program.

References

[1] E. Abbe, Arch. Mikrosk. Anat. **9**, 413 (1873).

[2] E. Betzig and J. K. Trautman, Science **257**, 189 (1992).

[3] A. Tselev, S. M. Anlage, H. M. Christen, R. L. Moreland, V. V. Talanov and A. R. Schwartz, Rev. Sci. Instrum. **74**, 3167 (2003).

[4] F. Zenhausern, Y. Martin and H. K. Wickramasinghe, Science **269**, 1083 (1995).

[5] R. Hillenbrandt, T. Taubner and F. Keilmann, Nature **418**, 159 (2002).

[6] M. I. Stockman, Phys. Rev. Lett. **93**, 137404 (2004).

[7] G. Lerosey, J. de Rosny, A. Tourin and M. Fink, Science **315**, 1120 (2007).

[8] P. C. M. Planken and N. C. J. van der Valk, Optics Lett. **29**, 2306 (2004).

[9] D. R. Smith, J. B. Pendry and M. C. K. Wiltshire, Science **305**, 788 (2004).

[10] D. R. Smith, Science **308**, 502 (2005).

[11] J. B. Pendry, Phys. Rev. Lett. **85**, 3966 (2000).

[12] N. A. P. Nicorovici, R. C. McPhedran and G. W. Milton, Phys. Rev. B **49**, 8479 (1994).

[13] G. W. Milton, N. A. P. Nicorovici, R. C. McPhedran and V. A. Podolskiy, Proc. Royal Soc. A **461**, 3999 (2005).

[14] R. Merlin, Appl. Phys. Lett. **84**, 1290 (2004).

[15] R. Shelby, D. R. Smith and S. Schultz, Science **292**, 77 (2001).

[16] A. Grbic and G. V. Eleftheriades, Phys. Rev. Lett. **92**, 117403 (2004).

[17] N. Fang, H. Lee, C. Sun and X. Zhang, Science **308**, 534 (2005).

[18] T. Taubner, D. Korobkin, Y. Urzhumov, G. Shvets and R. Hillenbrandt, Science **313**, 1595 (2006).

[19] See, e. g., E. Hecht, *Optics* (Addison Wesley, San Francisco, 2002)

[20] See, e.g., J. A. Stratton, *Electromagnetic Theory* (McGraw-Hill, New York, 1941); P. C. Clemmow, *The Plane Wave Spectrum Representation of Electromagnetic Fields* (Pergamon, Oxford, 1966).

[21] J. H. McLeod, J. Opt. Soc. Am. **44**, 592 (1954).

[22] J. Durnin, J. J. Miceli, Jr. and J. H. Eberly, Phys. Rev. Lett. **78**, 1499 (1987).

[23] D. R. Smith, D. Schuring, M. Rosenbluth, S. Schultz, S. A. Ramakrishna and J. B. Pendry, Appl. Phys. Lett. **82**, 1506 (2003).

[24] G. Shvets, Phys. Rev. B **67**, 035109 (2003)

Figure Captions

Fig. 1. Subwavelength focusing. (A) Two-dimensional case: $|F(y,z)|^2$ vs. y/ℓ from Eq. (3) where $F(y,0) \propto e^{iq_0 y}/(1+y^2/L^2)$ and $L/\ell = 2.5$. (B) Azimuthally-symmetric geometry: $|\Psi(\rho,z)|^2$ vs. $q_0\rho$ from Eq. (4) where $\Psi(\rho,0) \propto J_1(q_0\rho)/(1+\rho^2/L^2)$ and $L/\ell = 8$. The contour plots show the focal line (A) and ring (B) at $z = L$.

Fig. 2. Radiationless interference. (A) Schematic diagram showing a subwavelength plate, represented as a modulated array of linear current sources at $z = 0$ and the plane showing the focal line. $L/\ell = 3$; see Eq. (7). (B) Contour plot of $\ln|H_y|$. (C) Contour plot of $|H_y(z,y)/H_y(z,0)|^2$. The dashed white line at $z = L$ denotes the focal plane.

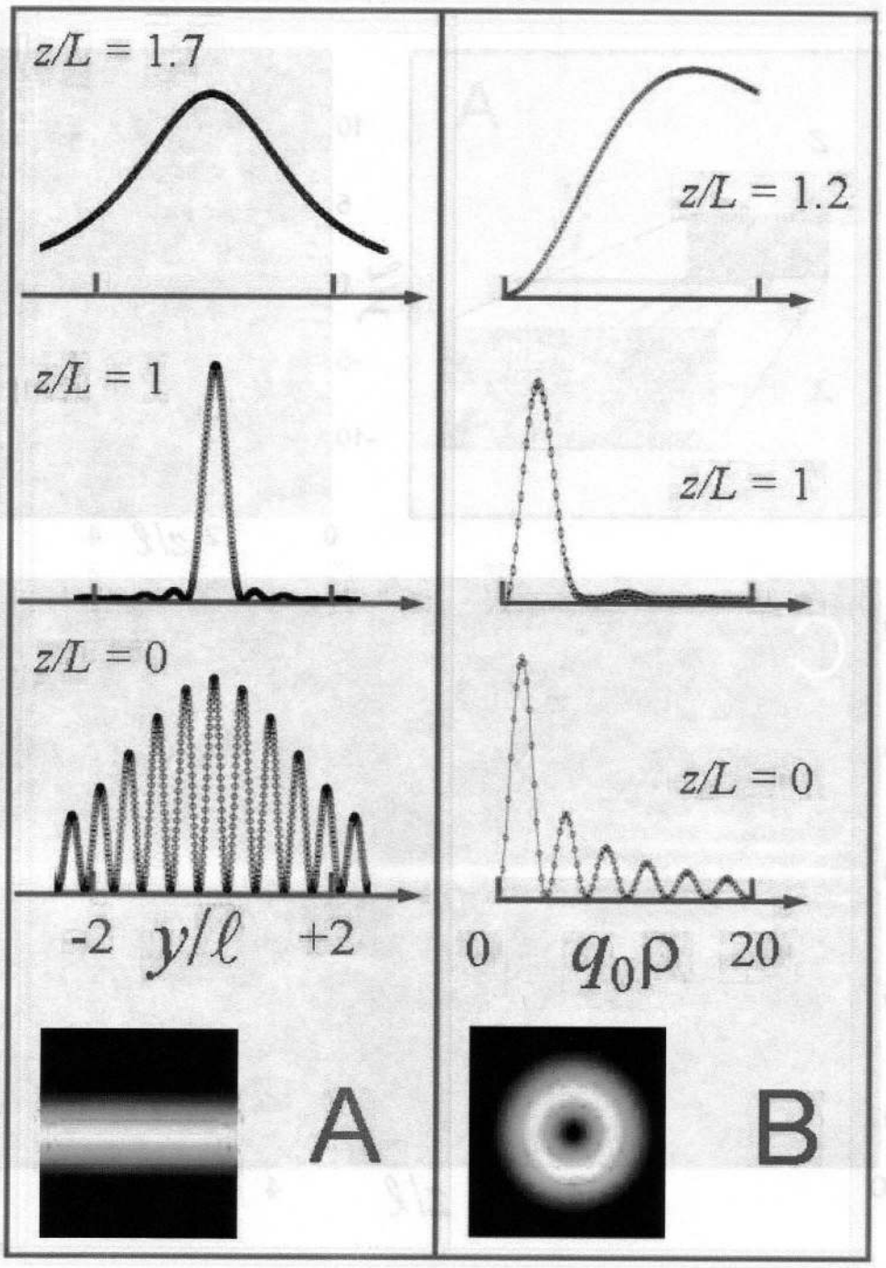

Figure 1

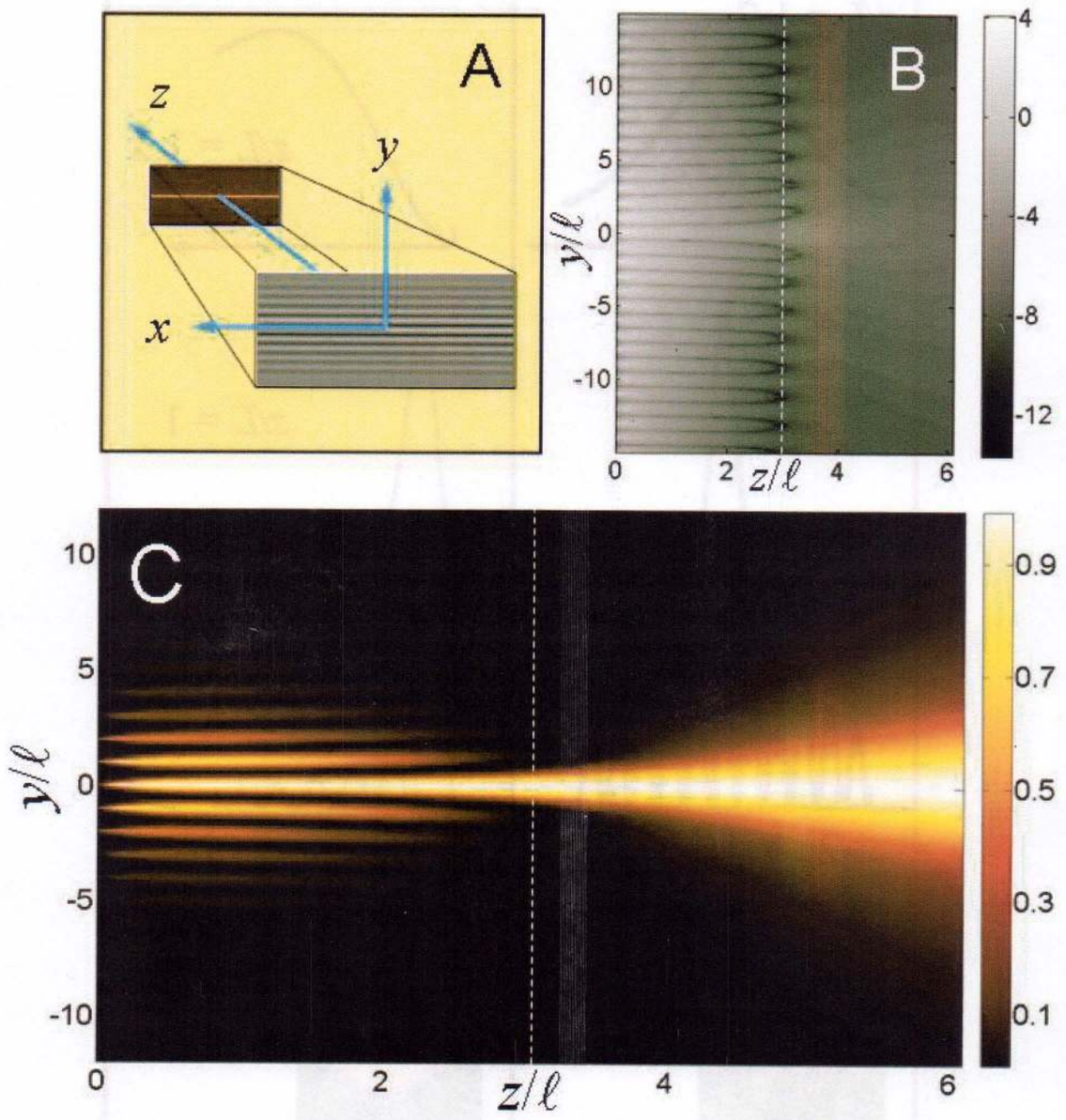
A
z
y
x
B
10
5
0
-5
-10
y/ℓ
0
2
z/ℓ
4
6
4
0
-4
-8
-12
C
10
5
0
-5
-10
y/ℓ
0
2
z/ℓ
4
6
0.9
0.7
0.5
0.3
0.1

Figure 2